Feedback Control of Wall Turbulence With Wall Deformation

Takahide Endo*1, Nobuhide Kasagi, and Yuji Suzuki

Department of Mechanical Engineering, The University of Tokyo,
Hongo 7-3-1, Bunkyo-ku, Tokyo, 113-8656, Japan
endo@thtlab.t.u-tokyo.ac.jp

Abstract

Direct numerical simulation of turbulent channel flow was made in order to evaluate feedback control with deformable walls. When the local wall velocity is determined by an active cancellation control scheme similar to Choi *et al.* (1994), the drag is decreased by about 12% with the wall deformation of the magnitude on the order of one viscous length. On the basis of the typical dimensions of the wall deformation thus obtained, a novel array of deformable actuators elongated in the streamwise direction is proposed. A new realizable control scheme by using wall information is developed based on physical arguments of the near-wall coherent structures. The location of quasi-streamwise vortices accompanied with streak meandering is successfully detected about 50 viscous length downstream from the sensing location, at which the spanwise gradients of wall shear stresses are measured. The wall velocity of each actuator is determined to counteract the wall-normal velocity induced by the streamwise vortices. By the present control scheme with the arrayed sensors and actuators, 10% drag reduction is achieved through selective manipulation of the streamwise vortices and streak meandering. It is also found that the energy input of the present control is one order of magnitude smaller than the pumping power saved.

Key Words: Turbulence control, DNS, Arrayed deformable actuators

*1 Present address: Computer and Information Division,
The Institute of Physical and Chemical Research (RIKEN)
Hirosawa 2-1, Wakou-si, Saitama, 351-0198, Japan. E-mail: tendo@postman.riken.go.jp

1. INTRODUCTION

Turbulence and concomitant phenomena such as heat transfer, diffusion, friction drag and noise play important roles in industrial and environmental problems. From the view point of saving power and protecting the environment, it is strongly desired to develop efficient turbulence control techniques for drag reduction and/or heat transfer augmentation. In the last three decades, various control strategies have been proposed (e.g., Bushnell & Hefner, 1990; Gad-el-Hak, 1994a). Among various methodologies, which are roughly classified into passive and active control, active feedback control attracts much attention because of its large control effect with small control input (Moin & Bewley, 1994; Gad-el-Hak, 1996; Kasagi, 1998).

Since 1960's, a considerlable degree of knowledge has been accumulated on the turbulent coherent structures and their underlying mechanism (e.g., Cantwell, 1981). Kline & Robinson (1989) grouped coherent motions observed in wall turbulence into eight classes. Among those coherent structures, quasi-streamwise vortices (QSV; hereafter) are known to play a dominant role in the near-wall turbulent transport phenomena (Robinson, 1991; Kasagi *et al.*, 1995). Jeong *et al.* (1997) proposed a conceptual model of the near-wall coherent structures, which consists of a train of QSVs having alternative signs of the streamwise vorticity. They also showed that QSV tilted in the spanwise direction have close relation with the meandering of low-speed streaks, and have major contribution to the regeneration mechanism. Kravchenko *et al.* (1993) showed that the streamwise vorticity accompanied with QSV has strong correlation with the wall shear stress upstream of the QSV. Kasagi & Ohtsubo (1992) found that the production and destruction of the Reynolds shear stress as well as the turbulence heat flux are concentrated in the regions close to QSV.

These facts indicate that an effective control of friction drag and/or heat transfer in wall turbulence can be established through selective manipulation of QSV.

Choi *et al.* (1994) investigated turbulent channel flow with local blowing/suction on the wall, which is opposite to the wall-normal velocity in the buffer layer. They obtained 30% drag reduction in their DNS, and found that QSV are attenuated. Bewley *et al.* (1993) employed a suboptimal control theory (Choi *et al.*, 1993) in order to determine the distribution of wall blowing/suction as the control input. They obtained 15% drag reduction and showed that the spatial distribution of blowing/suction determined by their suboptimal scheme is similar to that of Choi *et al.* (1994).

Lee *et al.* (1997) have developed a control algorithm based on neural networks. They determined the control input by using only wall variables, and found that the wall shear is substantially decreased when the blowing/suction rate is roughly proportional to the spanwise gradient of the spanwise shear stress. Lee *et al.* (1998) proposed a suboptimal control scheme with the Fourier transformation, and showed that their control scheme by using elaborate cost function is very effective in reducing drag.

It is noted that in most previous DNS studies for controlling wall turbulence, an infinite number of sensors and actuators were assumed, and their volumes were neglected. Since this assumption is unrealistic, it is desired to develop a new control algorithm assuming

arrayed sensors and actuators of finite spatial dimensions.

Devices for turbulence feedback control should have spatio-temporal scales comparable with those of the coherent structures (Gad-el-Hak, 1994b). Recent development of microelectromechanical systems (MEMS) technology enables us to fabricate prototypes of such micro devices (Ho & Tai, 1996). Among various kinds of actuators, wall deformation is considered to be one of the most promising candidates, because of its robustness against the hostile environment. Grosjean *et al.* (1998) fabricated pneumatic wall deformation actuators with MEMS techniques, and showed that these actuators survived transonic flight test with large temperature fluctuation.

Carlson & Lumley (1996) employed a Gaussian-shaped deformable bump as an actuator in their DNS of a minimal channel flow (Jiménez & Moin, 1991). They found that, when a bump having a maximum height of 12 viscous length and a maximum velocity of one friction velocity swells underneath the high-speed regions, the faster moving fluid is displaced away from the wall, and thus the friction drag is decreased as much as 7%. However, the effect of the wall motion on the near-wall coherent structures and the detailed friction drag reduction mechanism remain to be resolved.

Mito & Kasagi (1998) assumed sinusoidal wall oscillation uniform in the streamwise direction, of which amplitude and period is given by a predetermined way. They found in their DNS of a turbulent channel flow that the wall deformation induces long-term variation of wall friction, and makes low-speed streaks more stable and less meander in the spanwise direction during the time period when the friction drag is reduced. Their result indicates that the wall deformation should be effective in wall turbulence modification.

The objectives of the present study are to develop a new control algorithm based on the dynamics of near-wall coherent structure, which requires only wall variables, and to evaluate arrayed wall deformable actuators for drag reduction as a leading design of practical turbulent control devices. For this purpose, we employed DNSs of turbulent channel flow with deformable two walls.

2. NUMERICAL PROCEDURE

The flow geometry and the coordinate system are shown in Fig. 1. The governing equations are the incompressive Navier-Stokes equations and the continuity equation. Wall deformation is represented with a boundary-fitted coordinate system for moving boundary. Periodic boundary conditions are employed in the streamwise ($x-$) and spanwise ($z-$) directions, while non-slip boundary condition is imposed on the top and bottom deformable walls.

A modified Crank-Nicolson type fractional-step method (Choi & Moin, 1994) is used for the time advancement, while a second-order finite difference scheme is employed for the spatial discretization of both flow variables and metrics on a staggered mesh (Mito & Kasagi, 1998). The pressure Poisson equation is solved with the multi-grid method (Demuren & Ibraheem, 1998). Three levels of meshes are used to accelerate the convergence, in which a successive over relaxation (SOR) method is adopted in the finest and medium

meshes, whilst an incomplete LU conjugate gradient squared (ILUCGS) method is used in the coarsest mesh.

The size of the computational volume is respectively $2.5\pi\delta$ and $0.75\pi\delta$ in the $x-$ and $z-$ directions, where δ is the channel half width. The simulation is performed under the constant flow rate condition throughout the present study. The Reynolds number based on the bulk mean velocity U_b and the channel width 2δ is 4600 (about 150 based on the wall friction velocity u_τ and δ). The computational domain is about 1180 and 360 viscous length scales in the $x-$ and $z-$ directions, respectively, which are about 2.5 and 3.6 times larger than the minimal flow unit (Jiménez & Moin, 1991). Hereafter, $(\ )^+$ represents a quantity non-dimensionalized by the friction velocity u_τ in the plane channel flow without control and the kinematic viscosity ν.

The number of grid points is 96, 97 and 96 in the $x-, y-$ and $z-$directions, respectively. A non-uniform mesh with a hyperbolic tangent distribution is employed in the $y-$direction. The first mesh point away from the wall is given at $y^+ = 0.25$. The computational time step is chosen as $0.33\nu/u_\tau^2$. The initial condition is given from a fully-developed velocity field of preceding channel flow DNS.

3. ACTIVE CANCELLATION BY WALL DEFORMATION

In the first stage of the present study, a simple feedback algorithm similar to the v-control scheme (Choi *et al.*, 1994) is employed in order to evaluate the performance of wall deformation on drag reduction. The velocity of the wall deformation v_w is given to be out-of-phase of the wall-normal velocity in the buffer region; v_w at each grid on the deformable wall is determined as follows:

$$v_w^+(t_{n+1}) = -\left(v_s^+(t_n) - << v_s^+(t_n) >>\right) - 0.31 y_w^+(t_n), \qquad (1)$$

where t_n denotes time step n, while v_s is the wall-normal velocity at $y/\delta = 0.1$ ($y^+ \sim 15$). The second term is devised to keep the total volume of the flow domain constant, where the double bracket $<< \chi >>$ denotes an ensemble average of quantity χ in the $x-z$ plane at each time step. The third term of the RHS of Eq. (1) is a damping term to suppress excessive wall deformation, where y_w is the displacement of the wall.

Time trace of the drag coefficient normalized with its value for the uncontrolled plane channel flow is shown in Fig. 2. Note that the form drag of the deformable walls are found to be negligible, so the friction and total drags are employed synonymously in the present study. The friction drag is decreased to as large as 12% at $t^+ = 600$, and the mean drag reduction rate during $t^+ = 0 \sim 600$ is about 10%. Figure 3 shows an instantaneous shape of wall deformation. It is evident that the deformation is much elongated in the streamwise direction. Two-dimensional $(x-z)$ spectrum of the wall velocity v_w is shown in Fig. 4. Two marked peaks are observed at $(\kappa_x, \kappa_z) = (3,3)$ and $(5,5)$. Thus, the typical length scales estimated from these peaks are $(m_x^+, m_z^+) = (200, 60)$ and $(120, 36)$, where the spanwise scale is in between the mean diameter of QSV and the spacing of the near-wall streaky structures. As described later, dimensions of arrayed deformable actuators are determined based on these characteristic lengths.

Figure 2 also shows the rms value of the wall displacement is fairly small and is about $1.0\nu/u_\tau$. Wall roughness within $y^+ = 5$ is categorized as "hydraulically smooth" (Schlichting, 1960), and considered to have minor effect on the turbulent flow field. It is also noted that Goldstein & Tuan (1998) found in their DNS that the drag is slightly increased for the V-shaped riblet surface having $9\nu/u_\tau$ in height and $62.8\nu/u_\tau$ in spacing, of which spacing is close to the characteristic spanwise scale of the wall deformation obtained in the present study.

On the other hand, the rms value of the wall velocity is $0.15u_\tau$ and almost the same as that of the wall-normal velocity fluctuation at $y^+ = 10$. According to the v-control scheme by Choi *et al.* (1994), the optimal wall elevation of the sensor location is at $y^+ = 10$. Therefore, the drag reduction presently obtained should be due to the wall-normal velocity of the fluid induced by the wall deformation rather than the deformed shape of the wall.

4. DETECTION OF QUASI-STREAMWISE VORTEX BASED ON WALL VARIABLES

It is now evident that the wall deformation determined with appropriate control scheme is effective in drag reduction. In this section, a new algorithm to identify QSV based on the wall information is proposed from the argument on the dynamics of near-wall coherent structures.

It is well known that the near-wall streaky structures do not always flow straight in the streamwise direction, but often meander in the spanwise direction. Johansson *et al.* (1991) made a conditional average of a DNS database (Kim *et al.*, 1987) and found that the turbulent production was very large near the streaky structures asymmetric in the spanwise direction. Hamilton *et al.* (1995) pointed out that QSV and the streaky structure have close dynamical relationship with each other, and the meandering of streaks plays an important role in a quasi-cyclic process of turbulence regeneration. Jeong *et al.* (1997) proposed a schematic model of QSV alternatively tilting in the $x - z$ plane associated with the meandering of the near-wall low-speed streak. From the information mentioned above, it is expected that QSV can be identified from the wall information by detecting the streak meandering.

Figure 5 shows a schematic of a modelled streaky structure. When the velocity gradients in the two horizontal directions are taken into account, the edges of the streak can be grouped into four events as tabulated in Table 1, depending on the signs of $\partial u'/\partial x$ and $\partial u'/\partial z$. Note that E1 and E4, and also E2 and E3 are respectively of mirror symmetry in the spanwise direction.

In order to examine flow characteristics associated with each event, a conditional average of a plane channel flow is made, given the condition of the signs of $\partial u^+/\partial x^+$ and $\partial u^+/\partial z^+$ at $y^+ = 15$. A threshold of 0.32 is employed for both gradients to extract strong events only.

Figure 6 shows contours of the conditionally averaged streamwise velocity $< u'^+ >$ at $y^+ = 15$ for Events E1 and E2. The contours of negative $< u'^+ >$, which correspond to

the low-speed streaks, are elongated in the streamwise direction and tilted in the spanwise direction for both events. As depicted in Fig. 5, the detection point in E1 corresponds to the downstream edge of the low-speed streak, while that in E2 to the upstream edge.

Figure 7 shows contours of the conditionally averaged streamwise vorticity $< \omega_x^+ >$ at $y^+ = 15$ for Events E1 and E2. In Event E1, a large peak in $< \omega_x^+ >$ exists at the detection point. Thus, it is indicated that QSV having strong positive ω_x^+ often appears in Event E1. On the other hand, a negative peak in $< \omega_x^+ >$ is associated with Event E4 (not shown). For Events E2 and E3, the magnitude of $< \omega_x >$ is fairly small at the detection point. The present result is in accordance with the conceptual model proposed by Jeong *et al.* (1997) showing that QSVs are located on the downstream side of the meandering low-speed streaks.

The equation of the streamwise vorticity ω_x^+ is given as follows :

$$\frac{D\omega_x^+}{Dt^+} = \omega_x^+ \frac{\partial u^+}{\partial x^+} - \frac{\partial w^+}{\partial x^+}\frac{\partial u^+}{\partial y^+} + \frac{\partial v^+}{\partial x^+}\frac{\partial u^+}{\partial z^+} + \nabla^2 \omega_x^+, \tag{2}$$

where the first term of the RHS is the stretching term, while the second and third terms correspond to the tilting and twisting terms, respectively. Brooke & Hanratty (1993) showed that $(\partial w/\partial x) \cdot (\partial u/\partial y)$ is the largest in Eq.(2) near the wall, and ω_x is mainly produced by the tilting of ω_y in its early stage. Once ω_x is produced, however, the stretching term have substantial contribution (Sendstad & Moin, 1992). Since both $\partial u^+/\partial x^+$ and ω_x^+ are positive at Event E1, ω_x^+ is further produced by the stretching term $\omega_x \cdot (\partial u/\partial x)$, which results in the peak of ω_x^+ shown in Fig. 7(a). On the other hand, $\partial u^+/\partial x^+$ is negative for Event E2 while ω_x^+ is positive, so that the magnitude of ω_x^+ should be decreased. Thus, the streak meandering should contribute to the evolution of ω_x and hence the regeneration mechanism of QSV.

It is now clear that QSV accompanied with the meandering streaks can be detected by using $\partial u^+/\partial x^+$ and $\partial u^+/\partial z^+$ at $y^+ = 15$. In order to identify the meandering based on wall variables, we examined spatial relation between the streaks and the wall shear stress fluctuations. As a result, it is found that the spanwise gradients of τ_u^+ $(\equiv \partial u'^+/\partial y^+|_w)$ and τ_w^+ $(\equiv \partial w'^+/\partial y^+|_w)$ instead of the velocity gradients in the buffer layer are good indicators for the meandering streaks. The signs of the shear stress gradients and the corresponding events are summarized in Table 2. A negative value of $\partial \tau_w/\partial z$ is observed $50\nu/u_\tau$ upstream of Events E1 and E4, while $\partial \tau_w/\partial z > 0$ for E2 and E3. Note that Event E1 can be distinguished from E4 by the sign of $\partial \tau_u/\partial z$ at the same location.

Figure 8 shows the contours of the streamwise velocity fluctuation $< u'^+ >$ at $y^+ = 15$, conditionally averaged for S1 ($\partial \tau_u^+/\partial z^+ > 0.035$ and $\partial \tau_w^+/\partial z^+ < -0.005$). Although the tilting angle of the streak is slightly smaller than that shown in Fig. 6, the meandering of the low-speed streak corresponding to E1 is well captured at $50\nu/u_\tau$ downstream from the detection point. A large positive peak of ω_x^+ at $y^+ = 15$ is also observed in the same region, where the streak meanders as shown in Fig. 9. Although it is not shown here, a large negative peak of ω_x^+ is associated with S4 ($\partial \tau_u^+/\partial z^+ < -0.035$ and $\partial \tau_w^+/\partial z^+ < -0.005$), which corresponds to Event E4. Thus, QSV as well as its direction of rotation can be detected by the combination of the signs of $\partial \tau_u^+/\partial z^+$ and $\partial \tau_w^+/\partial z^+$.

Figure 10 shows contours of the conditionally averaged wall-normal velocity $< v'^{+} >$ at $y^{+} = 15$ for S1. Positive and negative peaks are aligned side-by-side in the spanwise direction, and they respectively correspond to the ejection and sweep motions. The spanwise distance of the positive and negative peaks is about $30\nu/u_\tau$, which is almost the same as the mean diameter of QSV (Robinson, 1991).

It is noted that the present control scheme based on the dynamics of the near-wall coherent structure is similar to the algorithm by Lee *et al.* (1997, 1998) in the sense that it requires $\partial\tau_w/\partial z$, although they employ different schemes such as a suboptimal control scheme and an adaptive control method based on neural network.

5. FEEDBACK CONTROL WITH ARRAYED DEFORMABLE ACTUATORS

In previous studies, sensors and actuators are assumed to be infinitely small, and placed at each computational grid point on the wall. In the present study, we assume control devices having finite dimensions, and design arrayed actuators and sensors based on the discussion descrived above.

Figure 11 (a) shows a schematic of deformable actuator assumed in the present computation. By taking into account the characteristic length of the wall deformation shown in Fig. 4, the streamwise and spanwise dimensions of the actuator is chosen as 172 and $60\nu/u_\tau$, respectively. Each actuator is assumed to be deformed only in the $y-$direction. The shape is determined with a sinusoid in the spanwise direction, in such a way that the distance between the peak and trough is about the mean diameter of QSV.

Figure 11 (b) shows an arrangement of arrayed shear stress sensors and deformable actuators. A shear stress sensor is assumed to be centered at $12.3\nu/u_\tau$ upstream from the upstream end of the deformable actuator. Hence, the streamwise distance between the sensor and the center of the actuator is $50\nu/u_\tau$, which corresponds to the displacement between the detection point of Events E1 and E4, and the peak of the streamwise vorticity shown in Fig. 9. In the present study, 36 actuators (6×6 in the streamwise and spanwise directions) are distributed with a regular pitch on both walls of the channel.

Each sensor measures the spanwise gradients of the instantaneous wall shear stresses, $\partial\tau_u/\partial z$ and $\partial\tau_w/\partial z$. The wall velocity at the center of the peak/trough of the actuator v_m is determined by:

$$v_m^+(t_{n+1}) = \begin{cases} \alpha \tanh\left(\dfrac{\partial\tau_u^+(t_n)}{\partial z^+}/\beta\right) - \gamma y_m^+(t_n), & \text{if } \dfrac{\partial\tau_w(t_n)}{\partial z} < 0, \\ -\gamma y_m^+(t_n), & \text{otherwise,} \end{cases} \tag{3}$$

where y_m is the wall displacement at the peak/trough, and α, β, and γ are control parameters, respectively. The wall velocity of each grid point on the actuator is given by

$$v_w^+(t_{n+1}) = v_m^+(t_{n+1}) \cdot f(x^+) \cdot \exp\left[-\frac{(z^+ - z_c^+)^2}{\sigma_z^{+2}}\right] \cdot \sin\left[\frac{2\pi\,(z^+ - z_c^+)}{m_z^+}\right], \tag{4}$$

where the function $f(x^+)$ is introduced to keep the shape of the actuator smooth in the streamwise direction. The function f is determined with a hyperbolic tangent as:

$$f(x^+) = \begin{cases} \frac{1}{2}\left[1 + \tanh\left\{\frac{(x^+ - x_c^+)+73.7}{\sigma_x^+}\right\}\right] & \cdots \text{if } -86 \le x^+ - x_c^+ \le -61.5, \\ 1 & \cdots \text{if } -61.5 \le x^+ - x_c^+ \le 61.5, \\ \frac{1}{2}\left[1 - \tanh\left\{\frac{(x^+ - x_c^+)-73.7}{\sigma_x^+}\right\}\right] & \cdots \text{if } 61.5 \le x^+ - x_c^+ \le 86. \end{cases} \tag{5}$$

In Eqs. (4) and (5), x_c and z_c denote the location of the center of the actuator. The parameters are somewhat tuned through preliminary computations, and chosen as $\alpha = 2.3, \beta = 0.077, \gamma = 0.3, \sigma_x^+ = 6.14$, and $\sigma_z^+ = 22.2$, respectively.

Figure 12 shows a time trace of the normalized pressure drop for the cases of local blowing/suction and the continuous wall deformation. It is seen the drag is gradually decreased from the onset of the control. The present result, however, exhibits no control effect until $t^+ = 200$, and then the drag is decreased at $t^+ > 200$. A maximum drag reduction rate of 17% is obtained at $t^+ = 800$. Therefore, even with coarsely distributed sensors and actuators on the wall, the effect of the present control scheme appears to be efficient through selective manipulation of QSV.

The gain in pumping power G and the energy input to deform actuators W_{in} are calculated to evaluate the performance of the present control. After Mito & Kasagi (1998), (i) work of convecting of turbulent kinematic energy, (ii) pressure work, and (iii) stress work, are taken into account as energy input, although the work for stretching the wall material is neglected.

$$G = \left[\left(\overline{-\frac{\partial p}{\partial x}}\right)_{\text{No-control}} - \left(-\frac{\partial p}{\partial x}\right)_{\text{Control}}\right] \cdot Q, \tag{6}$$

$$W_{in} = \int_{\Gamma_w} \left[\underbrace{p'_w \cdot v_n}_{\text{(i)}} + \underbrace{k \cdot v_n}_{\text{(ii)}} + \underbrace{\left(-\frac{1}{Re}\frac{\partial k}{\partial n}\right)}_{\text{(iii)}}\right] d\Gamma_w, \tag{7}$$

where Q, k and p'_w denote the flow rate, turbulent kinetic energy, and wall pressure fluctuation, respectively. The subscript n denotes wall-normal direction, and Eq. (7) is the surface integration over the deformable wall.

As shown in Fig. 13, the energy input for deforming actuators are much smaller than the pumping power saved. The mean efficiency $\eta(\equiv G/W_{in})$ is on the order of 10, and this fact demonstrates that the efficiency of the present control scheme with arrayed deformable actuators can be markedly large.

Figure 14 shows the top views of instantaneous flow fields at $t^+ = 0$ and 604. Vortical structures are identified with their negative value of the second invariant of the deformation tensor ($II' = u'_{i,j}u'_{j,i}$) (Chong *et al.*, 1990; Kasagi *et al.*, 1995). Under the present control with deformable actuators, QSV becomes less populated near the wall and the meandering of low-speed streak is surpressed.

The quadrant analysis (Lu & Willmarth, 1973) is employed to examine conditionally averaged flow field. The detection point is chosen at $y^+ = 15$, and the condition is given as:

$$|u'v'| \geq H u'_{\rm rms} v'_{\rm rms}, \tag{8}$$

where the threshold H is set to be unity.

Figure 15 shows the conditionally averaged streamwise velocity at $y^+ = 15$ associated with the ejection event. For all cases examined, a low-speed streak is clearly observed near the ejection event. Although each realization of the low-speed streak is elongated over a few thousand viscous length in the streamwise direction (Kline & Robinson, 1989), the conditionally averaged field exhibits much shorter structure because of the meandering in the spanwise direction. As shown in Fig. 15(b), the low-speed streak with the local blowing/suction becomes much shorter than that in the uncontrolled plane channel. On the other hand, under the present control with arrayed deformable actuators, it becomes longer in the streamwise direction. This fact indicates that the meandering of the streak is suppressed and the low-speed streak itself is much stabilized. Although it is not shown here, the two-point correlation of the streamwise velocity fluctuation persists longer in the streamwise direction as is often observed in drag reducing turbulent wall flows with polymer additives (Fortuna & Hanratty, 1972). Conditionally averaged displacement of the actuators near the ejection event shows that the actuators are deformed as a groove beneath the low-speed streaks. The groove follows the low-speed streak as it is convected downstream with keeping a depth of about $1\nu/u_\tau$.

This stabilization phenomenon of the low-speed streak is also shown in DNS of turbulent channel flow with sinusoidal wall oscillation uniform in the streamwise direction (Mito & Kasagi, 1998). Therefore, a possible drag reduction mechanism in the present control is that the breakdown process proposed by Hamilton *et al.* (1995) is surpressed, and the regeneration cycle of the near-wall turbulence vortex is hampered.

6. CONCLUSIONS

Direct numerical simulation of turbulent channel flow was made in order to evaluate feedback control with deformable walls. The following conclusions can be obtained:

1. Deformable wall can be an efficient actuator for wall turbulence with characteristic dimensions of 200 and 60 viscous lengths in the streamwise and spanwise directions, respectively. On the basis of this knowledge, a novel array of deformable actuators elongated in the streamwise direction is proposed.

2. A new simple control scheme is developed based on physical arguments of the near-wall coherent structures. The location of quasi-streamwise vortices accompanied with streak meandering is successfully predicted. Itis about 50 viscous length downstream from the sensing location, where gradients of wall shear stresses, $\partial\tau_u/\partial z$ and $\partial\tau_w/\partial z$, are measured.

3. About 10% drag reduction is achieved with arrayed sensors and actuators. The

streamwise vortices and streak meandering are selectively attenuated by the present control scheme. The energy input of the present control is one order of magnitude smaller than the pumping power saved.

References

Bewley, T.R., Choi, H., Temam R., and Moin P., 1993, "Optimal feedback control of turbulent channel flow," CTR Annual Research Briefs, Stanford Univ., pp. 3-14.

Brooke, J.W., and Hanratty, T.J., 1993, "Origin of turbulence-producing eddies in a channel flow," Phys. Fluids A, Vol. 5, pp. 1011-1022.

Bushnell, D. M., & Hefner, J. N., (eds.), 1990, Prog. Astronautics and Aeronautics: Viscous Drag Reduction in Boundary Layers, Vol. 123, AIAA.

Cantwell, B. J., 1981, "Organized motion in turbulent fnlow," Ann. Rev. Fluid Mech., Vol. 13, pp. 457-515.

Carlson, H.A., & Lumly, J.L., 1996, "Active control in the turbulent wall layer of a minimal flow unit," J. Fluid Mech., Vol. 329, pp. 341-371.

Choi, H., Temam, R., Moin, P., & Kim, J., 1993, "Feedback control for unsteady flow and its application to the stochastic Burgers equation," J. Fluid Mech., Vol. 253, pp. 509-543.

Choi, H., Moin, P., and Kim, J., 1994, "Active turbulence control for drag reduction in wall-bounded flows," J. Fluid Mech., Vol. 262, pp. 75-110.

Choi, H., and Moin, P., 1994, "Effects of the computational time step on numerical solutions of turbulent flow," J. Comput. Phys. Vol 113, pp. 1-4.

Chong, M. S., Perry, A. E., & Cantwell, B. J., 1990, "A general classification of three dimensional flow fields," Phys. Fluids A, Vol. 2, No. 5, pp. 765-777.

Demuren, A.O., and Ibraheem, S.O., 1998, "Multigrid method for the Euler and Navier-Stokes equations," AIAA J., Vol. 36, pp. 31-37.

Fortuna, G., and Hanratty, T. J., 1972, "The influence of drag-reducing polymers on turbulence in the viscous sublayer," J. Fluids Mech., Vol. 53, part 3, pp. 575-586.

Gad-el-Hak, M., 1994a, "Flow control," Appl. Mech. Rev., Vol. 42, No. 10, 261-293.

Gad-el-Hak, M., 1994b, "Interactive Control of Turbulent Boundary Layers: A Futuristic Overview," AIAA J., Vol. 32, No. 9, pp. 1753-1765.

Gad-el-Hak, M., 1996, "Modern developments in flow control," Appl. Mech. Rev., Vol. 49, pp. 365-377.

Goldstein, D. B, and Tuan, T.-C., 1998, "Secondary flow induced by riblets," J. Fluid Mech., Vol. 363, pp. 115-151.

Grosjean, C., Lee, G. B., Hong, W., Tai, Y.-C., and Ho, C.-M., 1998, "Micro Ballon Actuators for Aerodynamic Control," Proc. 11th MEMS Workshop, pp. 166-171.

Hamilton, J. M., Kim, J., and Waleffe, F., 1995, "Regeneration mechanism of near-wall turbulence structures," J. Fluid Mech., Vol. 287, pp. 317-348.

Ho, C-M., and Tai, Y-C., 1996, "Review: MEMS and Its Applications for Flow Control," ASME J. Fluids Eng., Vol. 118, pp. 437-447.

Jiménez, J., and Moin, P., 1991, "The minimal flow unit in near-wall turbulence," J. Fluid Mech., Vol. 225, pp. 213-240.

Jeong, J., Hussain, F., Schoppa, W., and Kim, J., 1997, "Coherent structures near the wall in a turbulent channel flow," J. Fluid Mech., Vol. 332, pp. 185-214.

Johanson, A.V., Alfredsson, P.H., and Kim, J., 1991, "Evolution and dynamics of shear-layer structures in near-wall turbulence," J. Fluid Mech., Vol. 224, pp. 579-599.

Kasagi, N., and Ohtsubo, Y., 1992, "Direct numerical simulation of low Prandtl number thermal field in a turbulent channel flow," Turbulent Shear Flows 8, Durst *et al.* eds., Springer-Verlag, Berlin, pp. 97-119.

Kasagi, N., Sumitani, Y., Suzuki, Y., and Iida, O., 1995, "Kinematics of the quasi-coherent vortical structure in near-wall turbulence," Int. J. Heat & Fluid Flow, Vol. 16, pp. 2-10.

Kasagi, N., 1998, "Progress in direct numerical simulation of turbulent transport and its control," Int. J. Heat & Fluid Flow, Vol. 19, pp. 125-134.

Kim, J., Moin, P., and Moser, R., 1987, "Turbulence statistics in fully developed channel flow at low Reynolds number," J. Fluid Mech., Vol. 177, pp. 133-166.

Kline, S. J., and Robinson, S. K., 1989, "Quasi-Coherent Structures in the Turbulent Boundary Layer: Part I," Status Report on a Community-Wide Summary of the Data. Near Wall Turbulence: 1988 Zaric Memorial Conference, Hemisphere.

Kravchenko, A. G., Choi, H., and Moin, P., 1993, "On the relation of near-wall streamwise vortices to wall skin friction in turbulent boundary layers," Phys. Fluids A, Vol. 5, No. 12, pp. 3307-3309.

Lee, C., Kim, J., Babcock, B., and Goodman, R., 1997, "Application of neural networks to turbulence control for drag reduction," Phys. Fluids, Vol. 9, pp. 1740-1747.

Lee, C., Kim, J., and Choi, H., 1998, "Suboptimal control of turbulent channel flow for drag reduction," J. Fluid Mech., Vol. 358, pp. 245-258.

Lu, S. S., & Willmarth, W. W., 1973, "Measurements of the structure of the Reynolds stress in a turbulent boundary layer," J. Fluids Mech., Vol. 60, part 3, pp. 481-511.

Mito, Y., and Kasagi, N., 1998, "DNS study of turbulence modification with streamwise-uniform sinusoidal wall-oscillation," Int. J. Heat & Fluid Flow, Vol 19, pp. 470-481.

Moin, P., and Bewley, T., 1994, "Feedback control of turbulence," Appl. Mech. Rev., Vol. 47, S3-S13.

Robinson, S.K., 1991, "Coherent motions in the turbulent boundary layer," Annu. Rev. Fluid Mech., Vol. 23, pp. 601-639.

Schlichting, H., 1960, "Boundary Layer Theory," McGraw-Hill, New York.

Sendstad, O., and Moin, P., 1992, "The near wall mechanics of three-dimensional turbulent boundary layers," Rep. TF-57, Dept. Mech. Eng., Stanford Univ.

Table 1. Four events at the edge of the meandering streaks.

Event	$\partial u'/\partial x$	$\partial u'/\partial z$
E1	Positive	Positive
E2	Negative	Positive
E3	Negative	Negative
E4	Positive	Negative

Table 2. Four signals and corresponding events.

Signal	$\partial \tau_u/\partial z$	$\partial \tau_w/\partial z$	Event	ω_x'
S1	Positive	Negative	E1	Positive
S2	Positive	Positive	E2	
S3	Negative	Positive	E3	
S4	Negative	Negative	E4	Negative

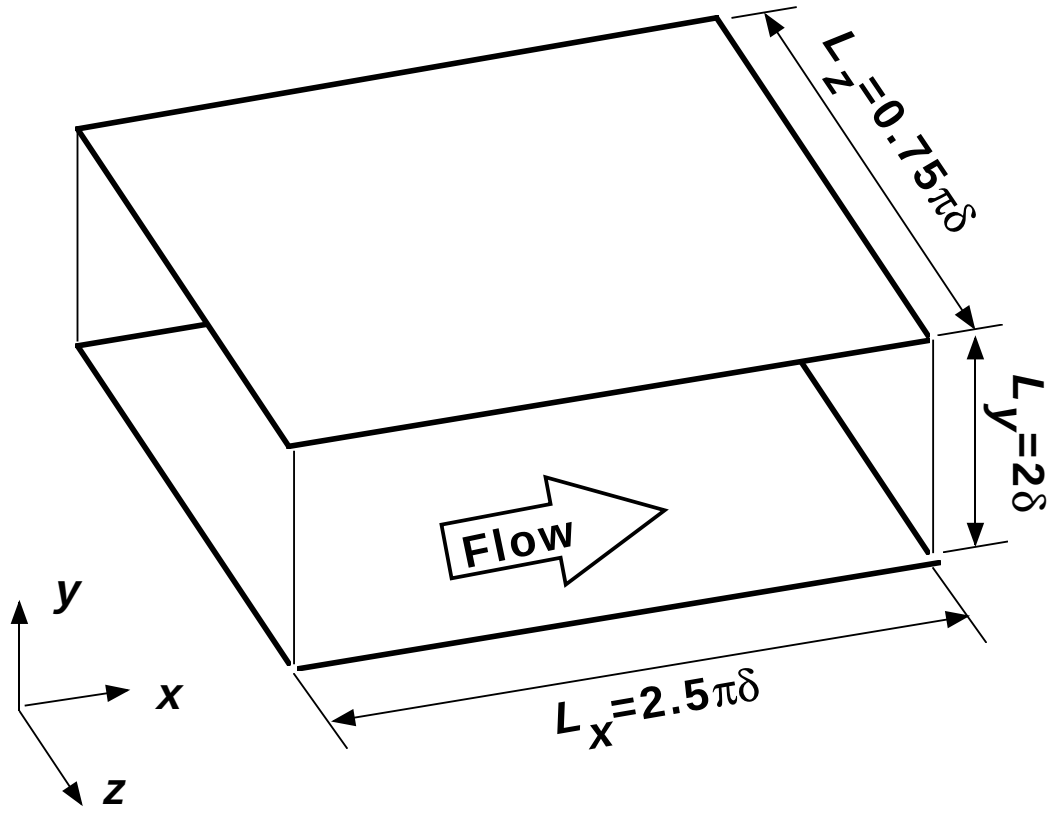

Figure 1. Flow geometry and coordinate system.

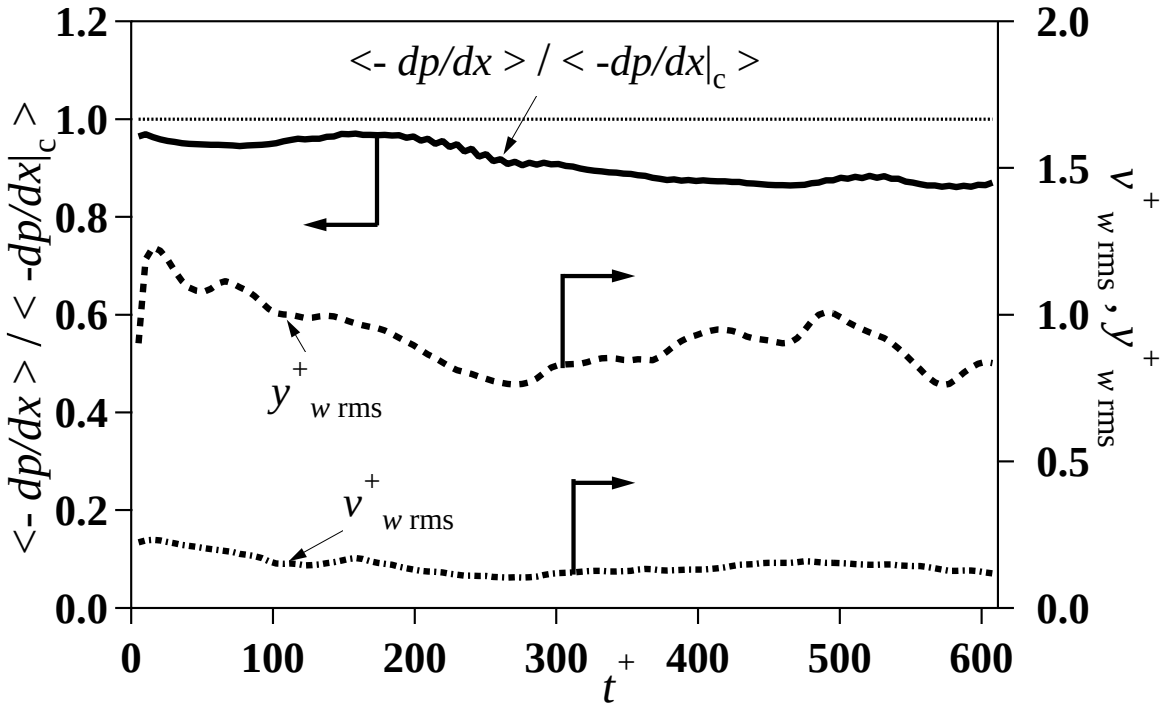

Figure 2. Time traces of the normalized mean pressure gradient and the rms values of y_w and v_w.

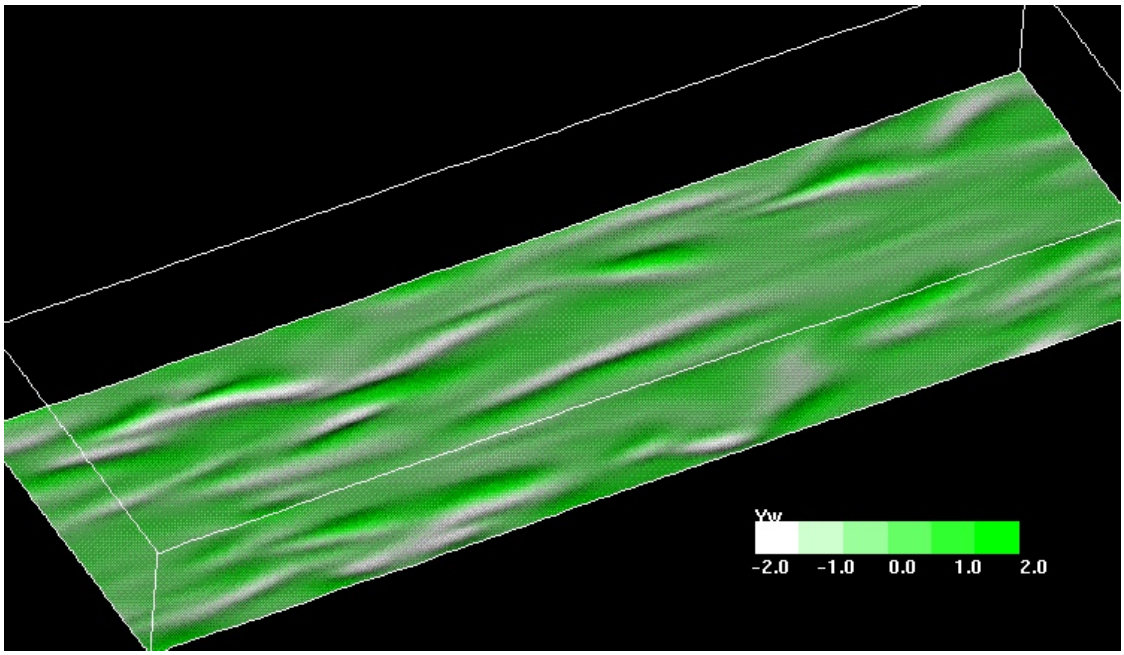

Figure 3. Instantaneous wall deformation ($t^+ = 5$). Flow : left to right, White to Green : $y_w^+ = -2$ to 2.

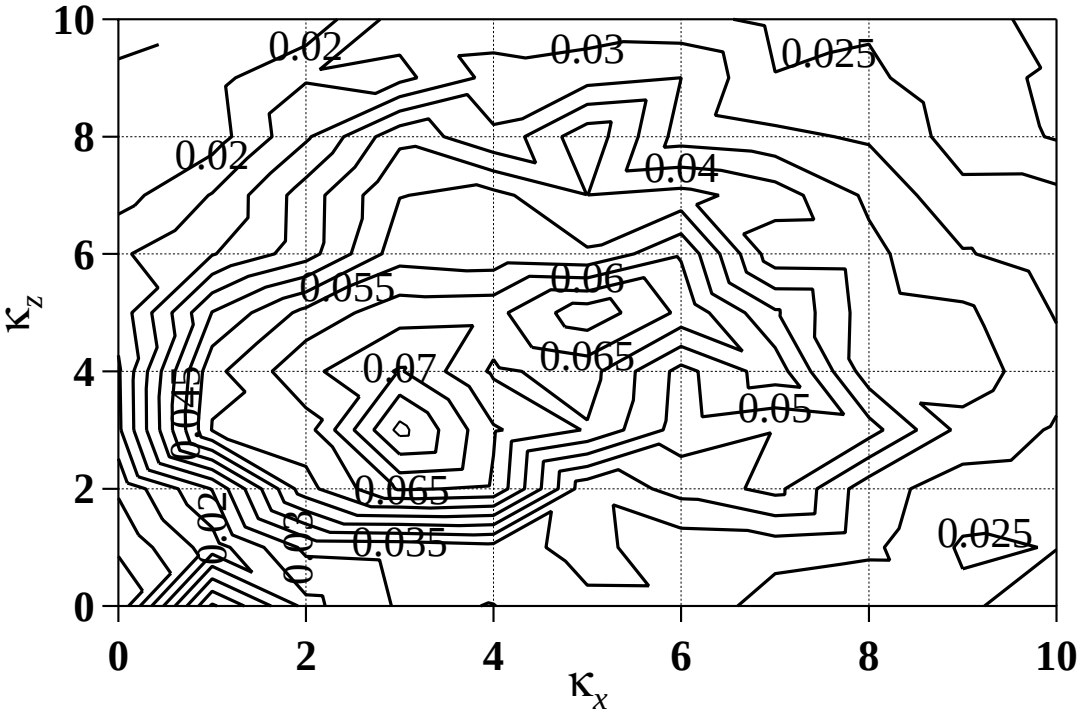

Figure 4. Two-dimensional spectrum of the wall velocity.

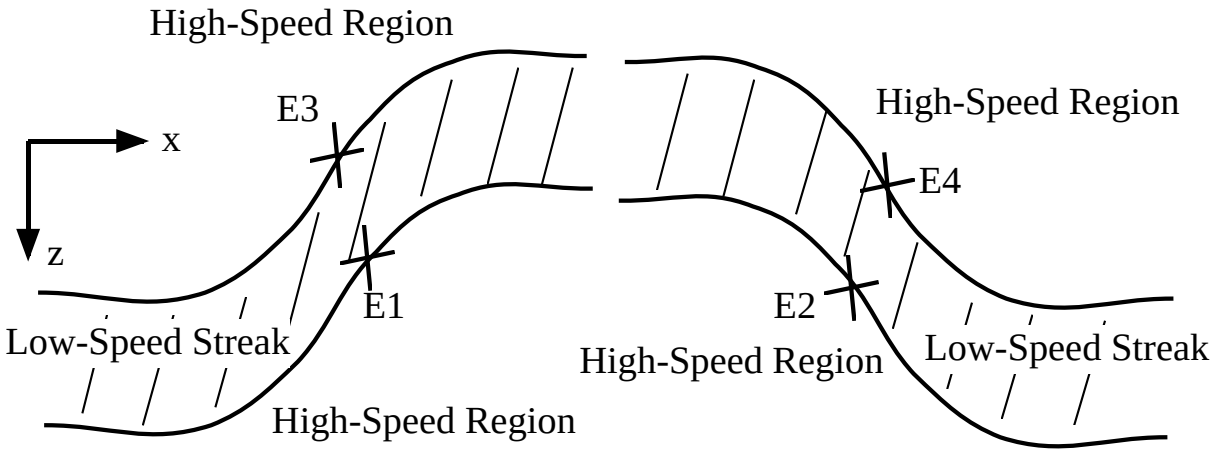

Figure 5. Schematic of a modelled streaky structure.

(a)

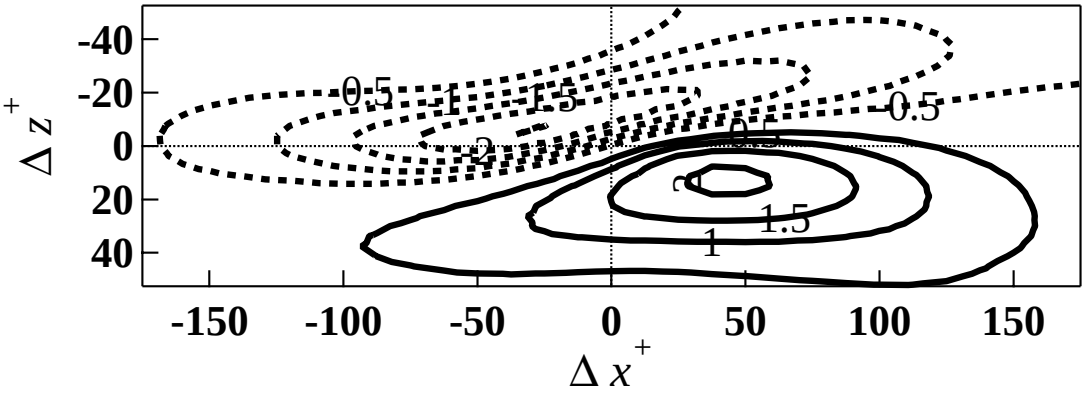

(b)

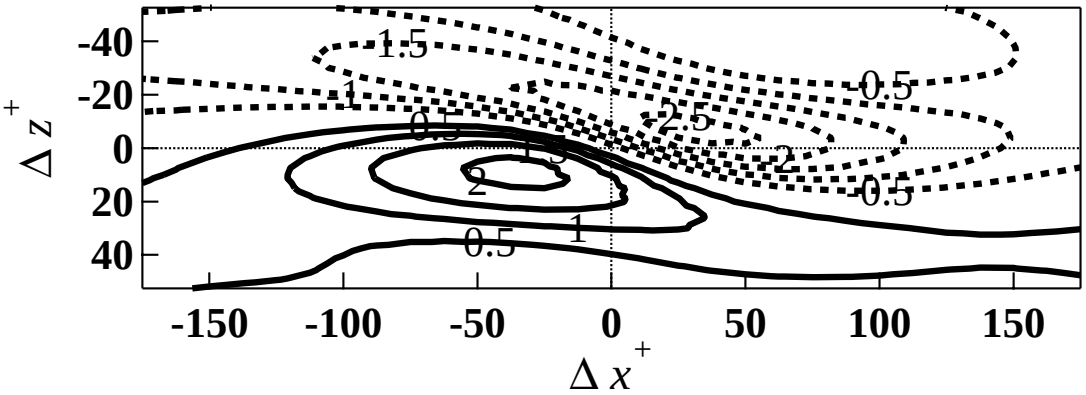

Figure 6. Contours of conditional-averaged streamwise velocity at $y^+ = 15$. The detection point is at $x^+ = 0$ and $z^+ = 0$. (a) Event E1, (b) Event E2.

(a)

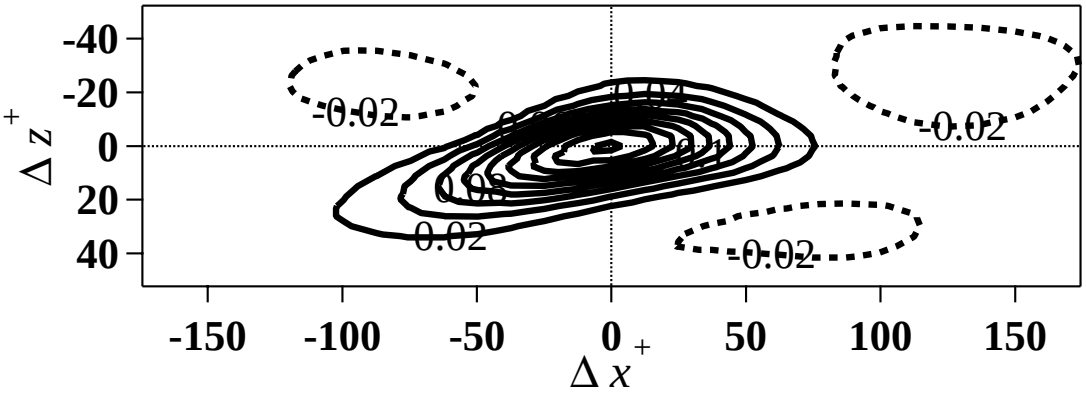

(b)

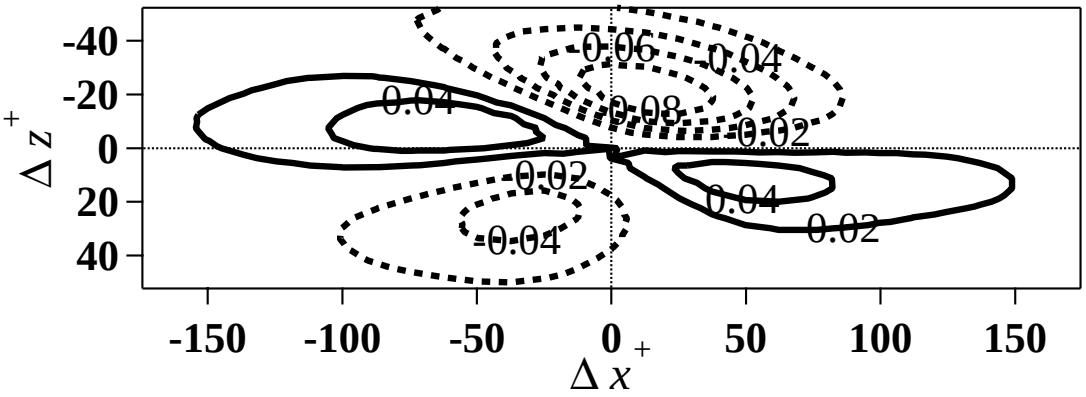

Figure 7. Contours of conditional-averaged streamwise vorticity at $y^+ = 15$. The detection point is at $x^+ = 0$ and $z^+ = 0$. (a) Event E1, (b) Event E2.

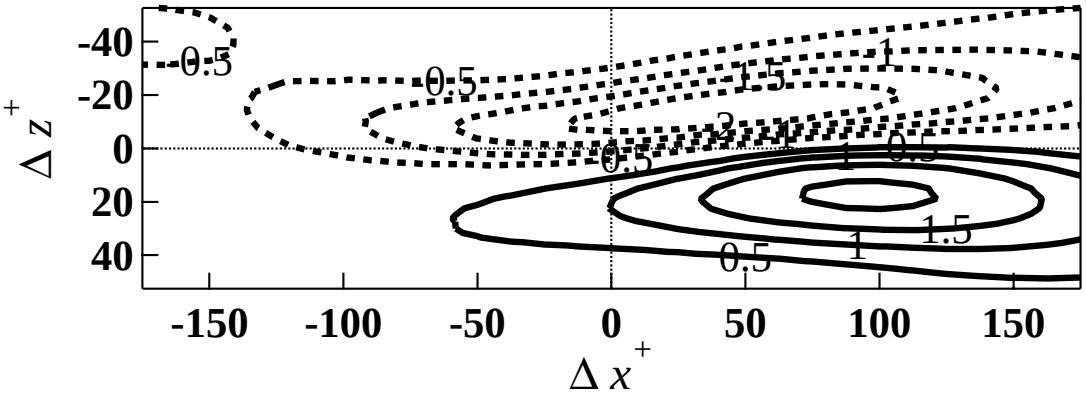

Figure 8. Contours of streamwise velocity at $y^+ = 15$, given the conditions of $\partial\tau_u^+/\partial z^+ > 0.035$ and $\partial\tau_w^+/\partial z^+ < -0.005$.

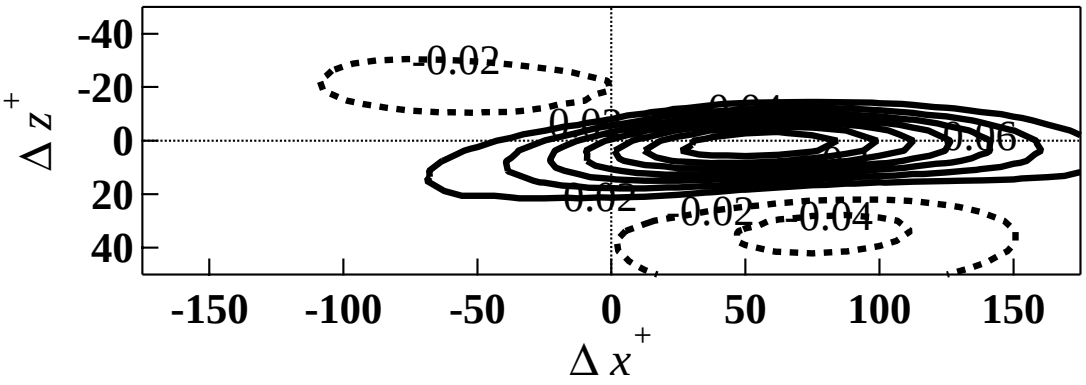

Figure 9. Contours of streamwise vorticity at $y^+ = 15$, given the conditions of $\partial\tau_u^+/\partial z^+ > 0.035$ and $\partial\tau_w^+/\partial z^+ < -0.005$.

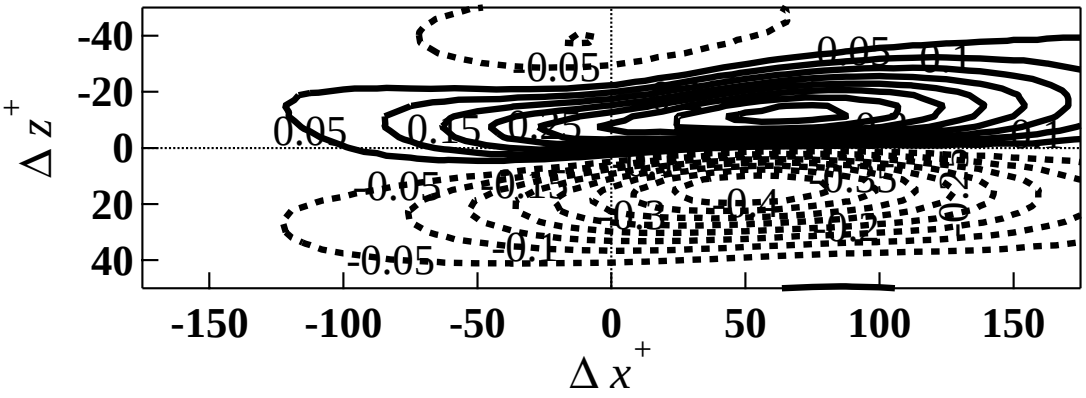

Figure 10. Contours of wall-normal velocity at $y^+ = 15$, given the conditions of $\partial\tau_u^+/\partial z^+ > 0.035$ and $\partial\tau_w^+/\partial z^+ < -0.005$.

(a)

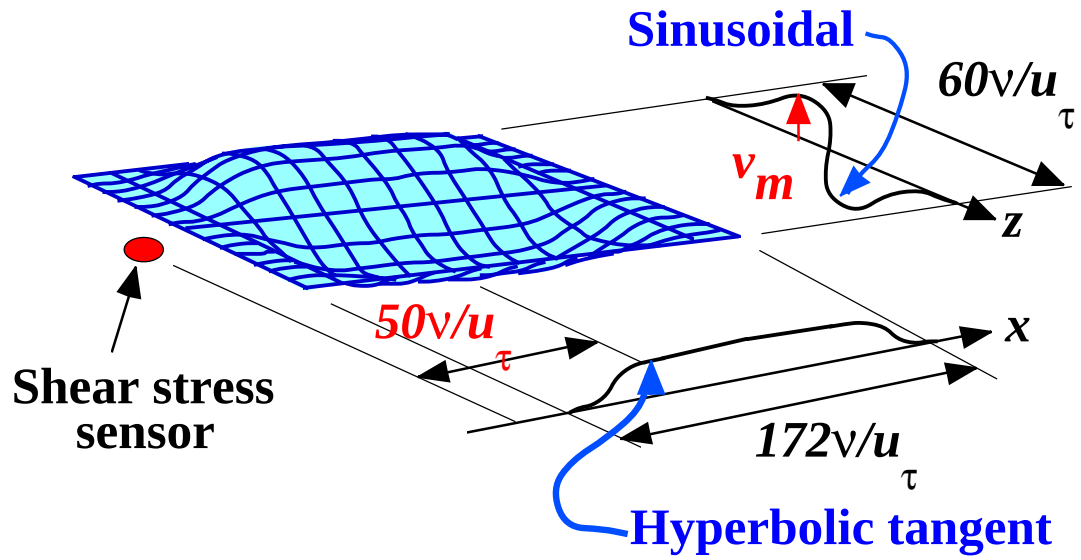

(b)

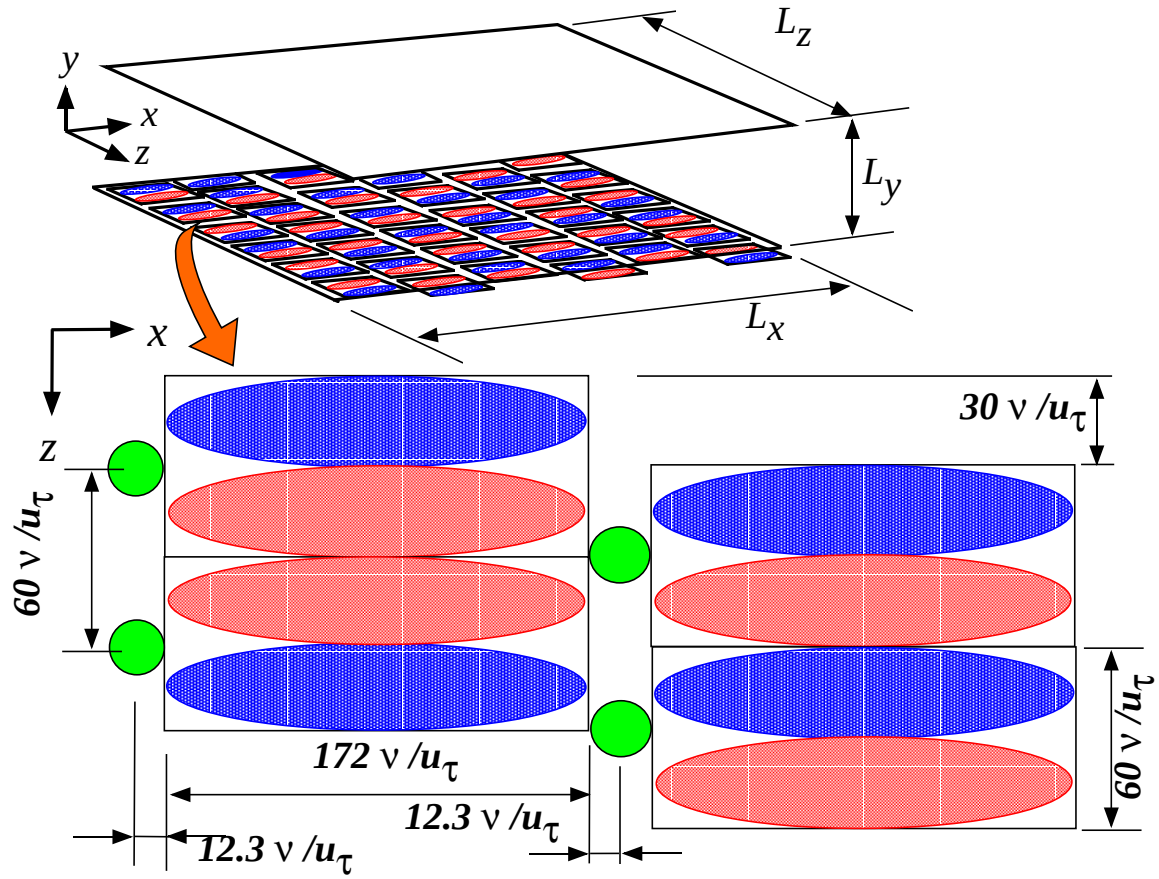

Figure 11. Schematic of arrayed actuators and shear stress sensors. (a) Dimension of a single deformable actuator. (b) Arrangement of the actuators and the sensors.

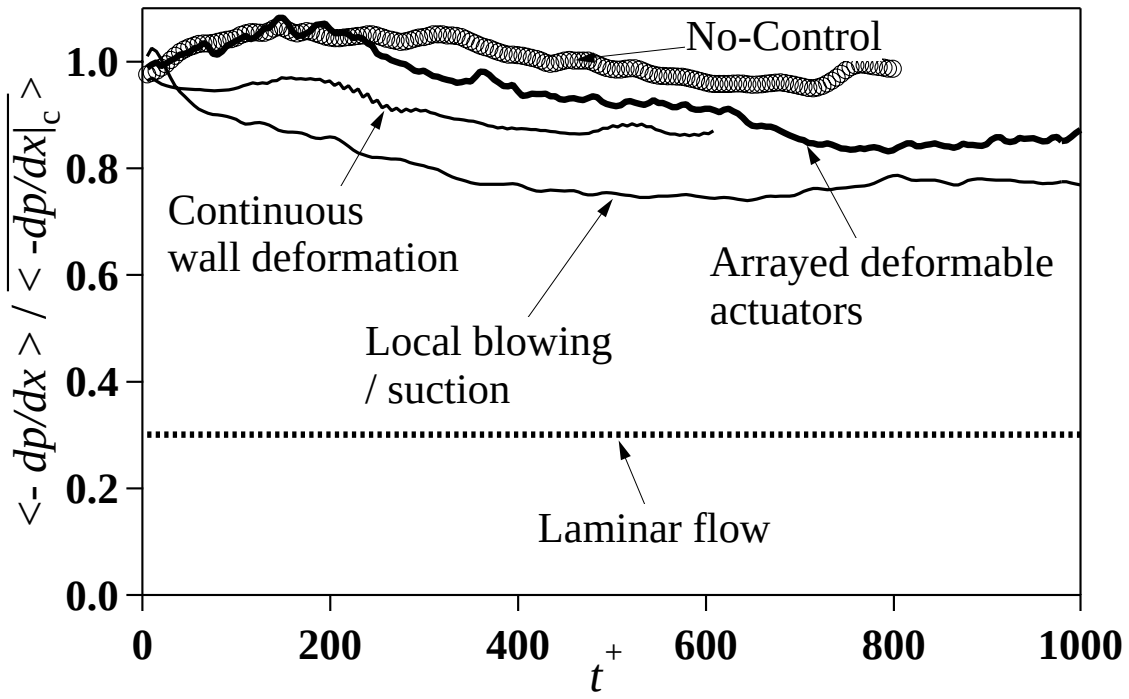

Figure 12. Time trace of the normalized mean pressure gradient.

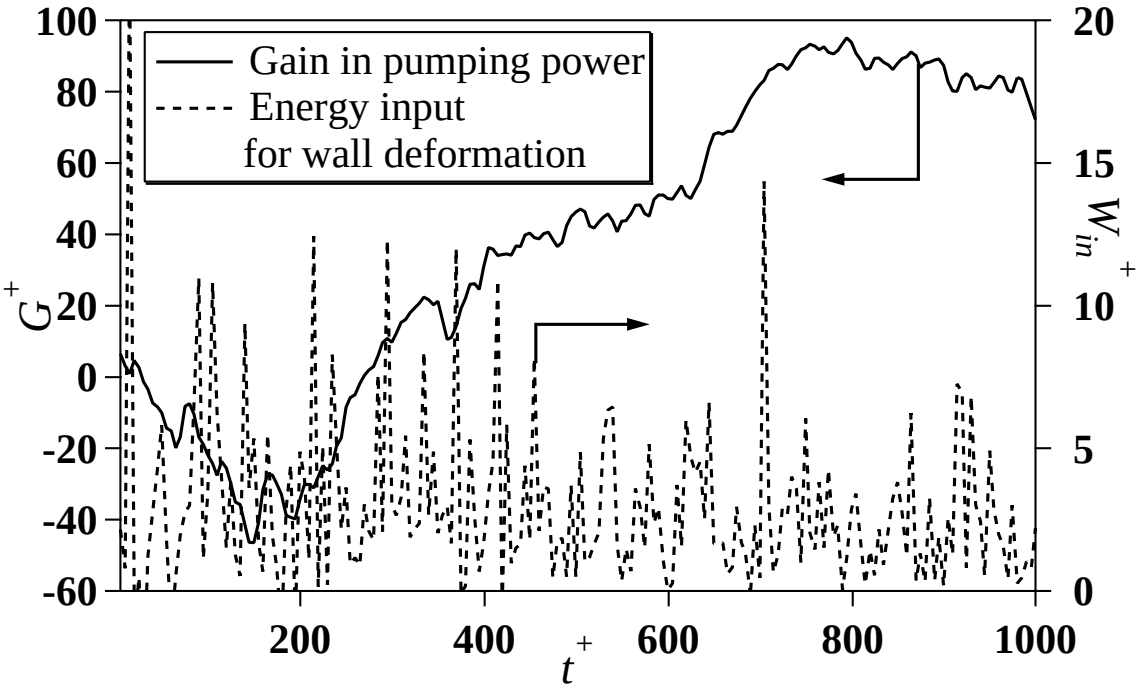

Figure 13. The gain in pumping work and the energy input.

(a)

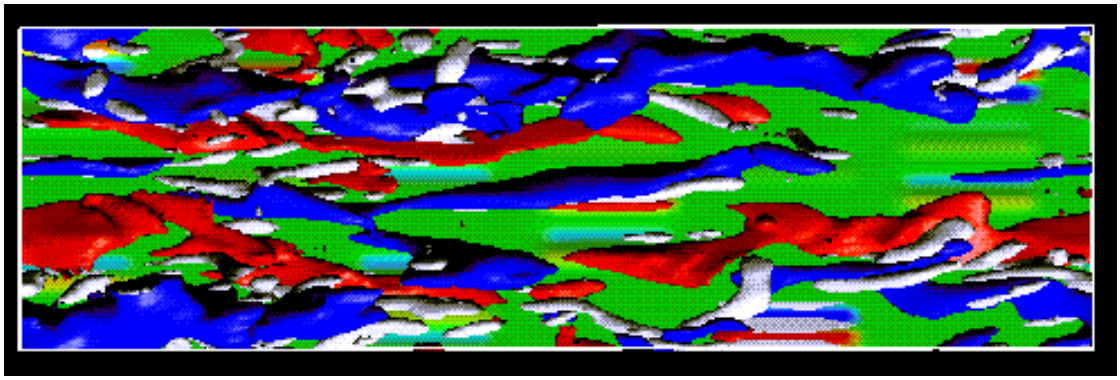

(b)

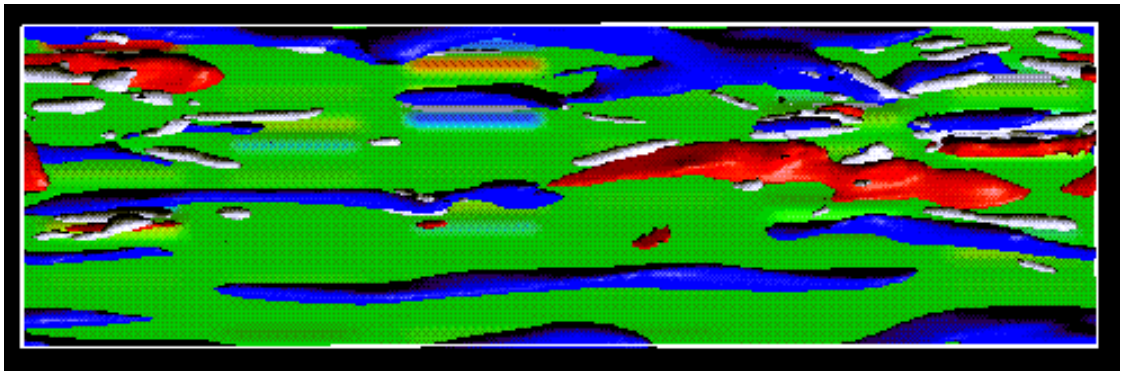

Figure 14. Top view of the instantaneous flow field. Flow: left to right. White: $II'^{+} = -0.03$, Blue: $u'^{+} = -3.5$, Red: $u'^{+} = 3.5$. (a) $t^{+} = 0$, (b) $t^{+} = 604$.

(a)

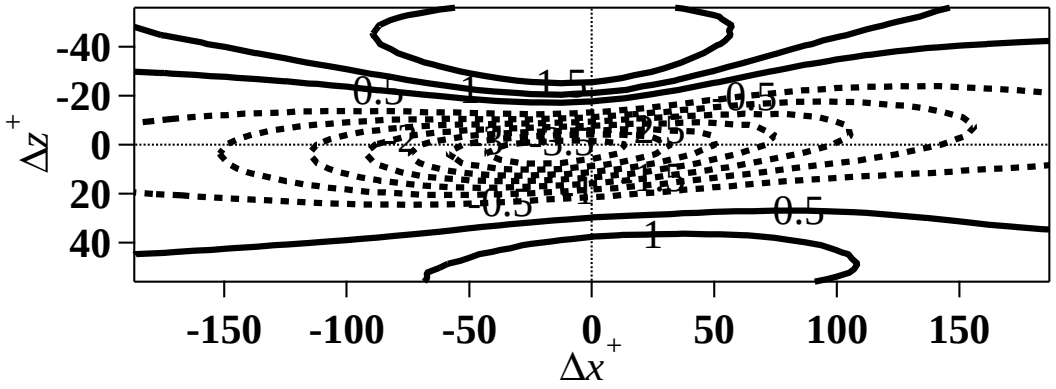

(b)

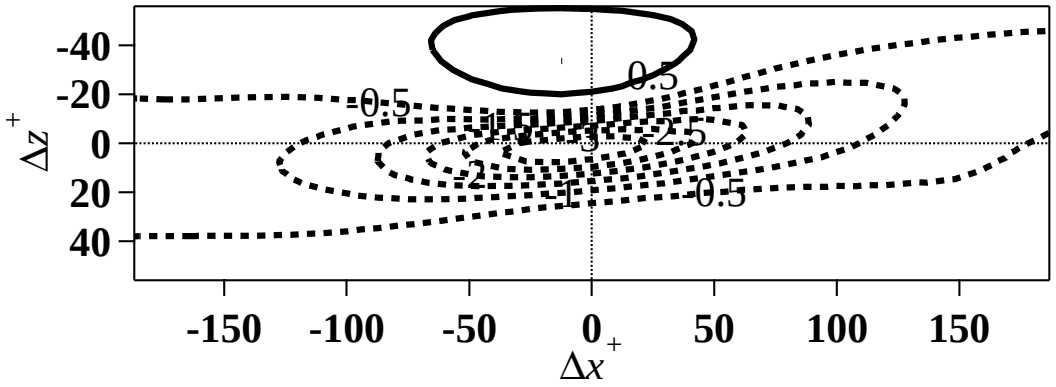

(c)

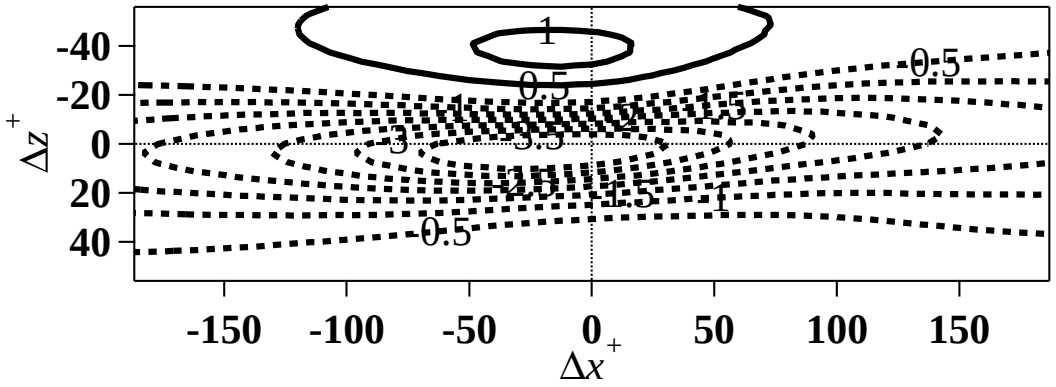

Figure 15. Conditional averaged streamwise velocity near the Q2 event. (a) No control, (b) Local blowing/suction, (c) Present results with arrayed deformable actuators.